Concrush: Understanding fugitive dust production and potential emission at a recycled concrete manufacturing facility

Brendan Florio[1] Fillipe Georgiou[2] Olivier D. Y. Huet[3]
Melanie E. Roberts[4] Matthew K. Tam[5]
Dimetre Triadis[6]

(Received 19 November 2020; revised 7 December 2021)

Abstract

The production and emission of fugitive dust is a topic of concern that Concrush brought to the MISG, 2020. Concrush is recycled concrete manufacturing company in the Hunter region of New South Wales. Concrush's operations produce fugitive dust, fine particles that can escape the site. Fugitive dust can travel long distances from the site of emission, and can have negative health impacts including respiratory illnesses. Presently, concrete recycling facilities are managed by the Environmental Protection Agency using guidelines initially developed for the coal industry. Concrush seeks to understand the appropriateness

DOI:10.21914/anziamj.v62.15997, Published 2022-03-16, as part of the Proceedings of the 2020 Mathematics and Statistics in Industry Study Group. ISSN 1445-8810. (Print two pages per sheet of paper.)

of these guidelines, and how they can reduce and manage fugitive dust on their Teralba site. Mathematical modelling of dust emission and transport, together with a review of similar processes in the literature, identified a number of practical options for Concrush to reduce their dust emissions. In addition, opportunities for improved data collection are identified.

Subject class: 76-10

Keywords: dust; erosion; air quality

Contents

1 Introduction and problem description

Concrush is a concrete recycling operation located in Teralba in the Hunter region of New South Wales that takes in concrete waste and crushes it. The crushed product is then on-sold as road-base, drainage aggregate, and perhaps in the future, aggregates to produce recycled concrete. The targeted size of the crushed product is determined by its intended use. For example, drainage aggregate measures up to 20 mm, whereas road-base requires a spectrum of particle sizes as a mix of course and fine aggregate allows the desired compactability properties. As a by-product of this concrete processing, very fine "fugitive" dust particles are produced, which can become airborne and contribute to poor air quality.

While air quality in the Hunter region has historically been a problem (Higginbotham et al. 2010), it was not until 2013 that the air quality was assessed in the upper region (Hibberd et al. 2013) and 2016 for the lower region (Hibberd et al. 2016). Based on these assessments the NSW Environmental Protection Authority (EPA) have set limits on the amount of fine particles generated at industrial sites such as Concrush. As a small business of the Hunter community, Concrush is driven to reduce the emission of fugitive dust for both regulatory reasons and a sense of community responsibility. Currently, Concrush maintain four dust gauges on the perimeter of the site. These are analysed monthly for fine dust content to give an insight into their dust emissions.

The guidelines imposed on Concrush by the EPA are the same as those that are imposed on the coal industry. However, coal and concrete dust are different. Critically, coal dust is typically of much lower density than concrete dust, which affects transport and settling. Concrush are seeking external guidance by the Maths in Industry Study Group to investigate the appropriateness of these regulations for a concrete recycling plant. If they are too strict, then they may unduly effect the productivity of the site. If they are too loose, then significant dust generation may occur despite regulatory approval.

Irrespective of the EPA requirements, Concrush are seeking greater insight into the production and dispersion of dust to drive suppression strategies. Based on the overall context, we distilled the problem into three main questions: What are the critical processes that produce airborne dust and how much do they produce? For the dust in the perimeter gauges, what can be attributed to Concrush as opposed to the surrounding industries? And once the dust is produced, where does it go? We chose to address these problems by looking at the available literature in Section 2, data analysis in Section 3, and mathematical modelling in Sections 4 and 5.

2 Literature review

To begin, the "fugitive" particles of interest fall into two categories: PM10 and PM2.5, corresponding to particles of diameter $< 10\,\mu m$ and $< 2.5\,\mu m$ respectively. Particles that span less than $10\,\mu m$ are able to invade the upper airways and can cause irritation, while particles that span less than $2.5\,\mu m$ are able to penetrate the lower airways and even enter the bloodstream, often carrying a toxic payload (Xing et al. 2016). One study by Pope et al. (2002) found that each increase of $10\,\mu g/m^3$ of PM2.5 lead to 4% increase in general mortality, 6% increase in cardiopulmonary related deaths, and an 8% increase in lung cancer related deaths. A more recent study of over 68 million US medicare enrollees found that a decrease in PM2.5 by $10\,\mu g/m^3$ leads to a statistically significant 6% to 7% decrease in mortality risk (Wu et al. 2020). Due to their small size, PM2.5 particles are also able to remain airborne for extended periods and thus travel long distances from their source.

Within the Concrush site, the main sources of these fugitive dust particles are the crushing and grinding processes, the erosion of fine dust from aggregate stockpiles and unsealed roads, and wheel-lifted dust from the transit of large vehicles over unsealed roads. In order to study the effect of these sources we turned to the available literature and found there have not been studies about fugitive dust and the concrete recycling process. With this in mind we

investigated the fugitive dust caused by the processing of similar materials, namely rock and gravel: Petavratzi, Kingman, and Lowndes (2005) reviewed these processes.

While the crushing of concrete is the only process that actually produces fine particles, the emission of fugitive dust in crushing is quite low as the process is well-shielded (Chang et al. 2010).

Stockpiles have the potential to be a significant source of fugitive dust. Background wind draws fine particles out of stockpiles, so the emission of dust increases with increasing wind speed. However, this emission only starts above some threshold value (Diego et al. 2009; Xuan 2004). This emission is also affected by many factors including pile shape and material size (Toraño et al. 2007). Building barriers, ranging from simple wind-breaking cloth to a fully enclosed building, to reduce wind speed across the site, has a large effect on reducing these emissions (Toraño et al. 2009; Ferreira and Lambert 2011). In addition, wetting material stockpiles during high winds works to lower emissions by increasing threshold friction velocity. It is also possible to arrange stockpiles such that piles of coarse aggregate act as a windbreak to protect piles of fine aggregate (Badr and Harion 2007). However, such arrangements need to take seasonal dominant winds into account as moving material around the site, with dumping in particular, causing moderate fugitive dust emissions (Petavratzi, Kingman, and Lowndes 2005).

Truck movement within the site, particularly over unsealed roads, which have emission factors up to 75 times higher than their sealed counterparts (Claiborn et al. 1995), are possibly the largest source of emissions (Chang et al. 2010). The floor of the site becomes covered by accumulated fine particles that have conveniently settled, truck movement disturbs these fine particles and can send them into the air as fugitive dust. Some methods to limit these emissions include changing to sealed roads and regular wetting of the roadway (Watson, Chow, and Pace 2000).

Screening is a process whereby crushed aggregate is passed through a series of agitated sieves with progressively finer grading, which acts to sort the aggre-

gates. As this is a mechanically energetic process, fine particles may become airborne and escape as fugitive dust. The inclusion of control techniques such as wetting and physical barriers can reduce the emission factor by an order of magnitude (US EPA 1995; Sairanen, Rinne, and Selonen 2017).

Once airborne, wind is the most significant factor in the transport of dust (Wark, Warner, and Wayne T. 1998). Due to this factor, Concrush cease all dust producing operations if the local wind speed exceeds $18\,\mathrm{km\,h^{-1}}$ ($5\,\mathrm{m\,s^{-1}}$). Any method to reduce the wind speed by arranging windbreaks would go a long way to reduce dust emissions, due to its relationship with both emission and transport (Stunder and Arya 1988). At the moment, the Concrush site is completely open, so this is an easy area for improvement. To better understand how these particles move once airborne we looked at mathematical modelling in Sections 4 and 5.

In the immediate area there are additional sources of dust including a freight line where coal is transported, a high traffic main road, and a former lead mine. In order to understand their impact on the site we turn to data analysis in Section 3.

3 Data analysis

A variety of onsite and offsite data sources were explored. For regulatory reporting, the Concrush site contains four dust deposition gauges, each located at a different corner of the site boundary. This type of dust gauge passively collects dust via a funnel into a bottle, which is sent to a laboratory for gravimetric analysis approximately every 30 days. As this technique can only report monthly aggregates, it does not allow dusts levels from specific onsite events to be determined. Consequently, it is difficult to draw any meaningful data from the onsite dust deposition gauges and we looked further for useful data.

The Department of Planning, Industry and Environment publish pollutant

Figure 1: Average PM10 and PM2.5 concentrations at offsite reporting stations in the Lower Hunter by time of day for the period 2014–2019. The shading around each series represents a 95% confidence interval.

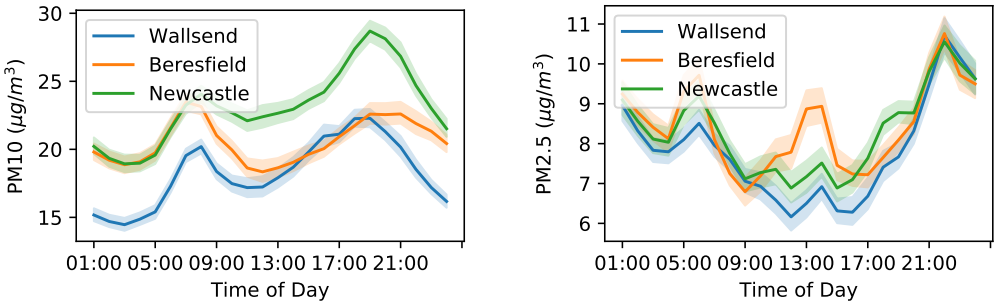

and meteorological information at a number of sites located across New South Wales (*Department of Planning, Industry and Environment's Data Download Facility*). This data includes hourly averages for PM10 and PM2.5 concentrations at three offsite stations located in the Lower Hunter region, including one (Wallsend) within 10 km of the Concrush site, which was used to study background dust in the area. Using data for the five year period of 2014–2019, we examined the time of day average concentrations of PM10 and PM2.5 particles. The resulting plot for PM10 (Figure 1) is bimodal with distinct peaks at about 8 am and 6:30 pm, which we conjecture corresponds to peak hour traffic times. No such peaks were observed in the corresponding PM2.5 data (Figure 1).

3.1 Onsite data provided by Concrush

Concrush provided selected onsite aerosol concentration data obtained by third-party contractors in 2014 and 2020. Measurements were recorded regularly at five minute intervals for extended periods of time. Data collected at different times show surprising qualitative and quantitative differences that

Figure 2: Average PM10 and PM2.5 concentrations at the Wallsend reporting station for the three time periods considered in Section 3.1. The shading around each series represents a 95% confidence interval.

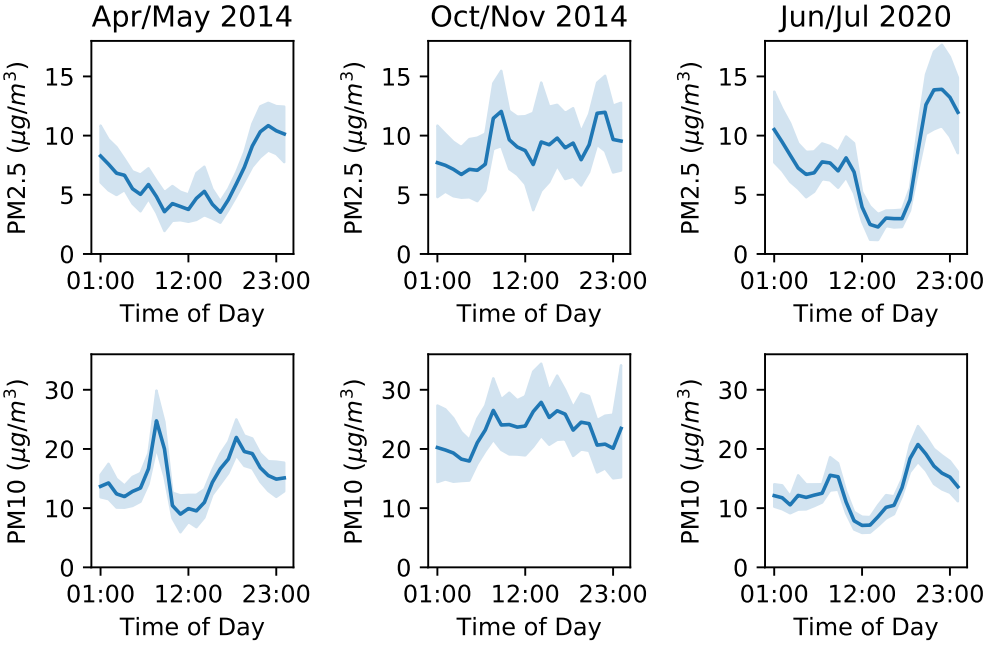

are explored below. Detailed data of truck arrivals and departures have also been provided for periods of interest in 2014 and 2020. These truck movements are likely to generate some dust, and also provide an approximate indication of other worksite activity that is likely to cause dust. The number of times a truck is recorded entering or exiting the worksite every five minutes is used to supplement selected aerosol concentration data below. The corresponding off-site (Wallsend) aerosol measurements for periods of interest are shown in Figure 2. This figure suggests that the off-site aerosol concentration behaved similarly in Apr/May 2014 and Jun/Jul 2020, with PM2.5 peaking at night and PM10 peaking in the morning and late afternoon. In contrast, these

Figure 3: Overview of PM10 aerosol data provided for 2014. Several device interruptions are indicated with blue dashed lines.

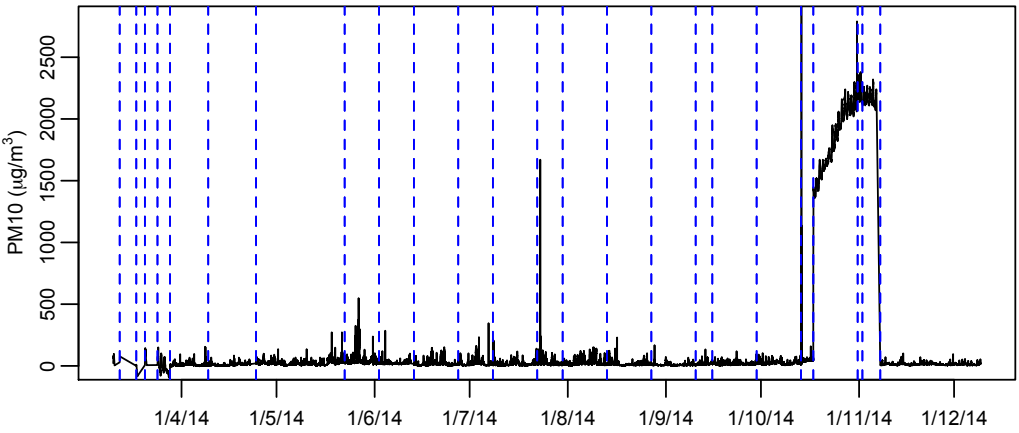

peaks did not clearly appear in the aerosol concentration in Oct/Nov 2014 which was more disperse.

Figure 3 shows an overview of the 2014 aerosol concentration measurements ($\mu g/m^3$). Data was collected using a TSI Dust Trak Model 8520 Aerosol Monitor that measures PM10 particle concentrations with a listed particle size range of 0.1 to 10 µm. Here aerosol concentrations are estimated using a light-scattering laser diode. Several device collection interruptions of varying lengths are apparent in the logged data, and are indicated with dashed blue lines in Figure 3. The third-party contractor responsible for the operation of the Dust Track device submitted their first aerosol summary report for the month of April 2014. The data for March 2014 with protracted device interruptions and apparent negative values is hence assumed to be invalid, likely corresponding to initial device setup and calibration.

Data recorded for the late half of October and early November is clearly of a different character to data recorded at other times. In the original data summary report, the October/November data was said to be affected by

Figure 4: Truck traffic displayed above aerosol data recorded without interruption in April and May 2014. The number of trucks entering or exiting the worksite during five minute intervals are plotted in blue. Dashed lines show 24 hour moving averages.

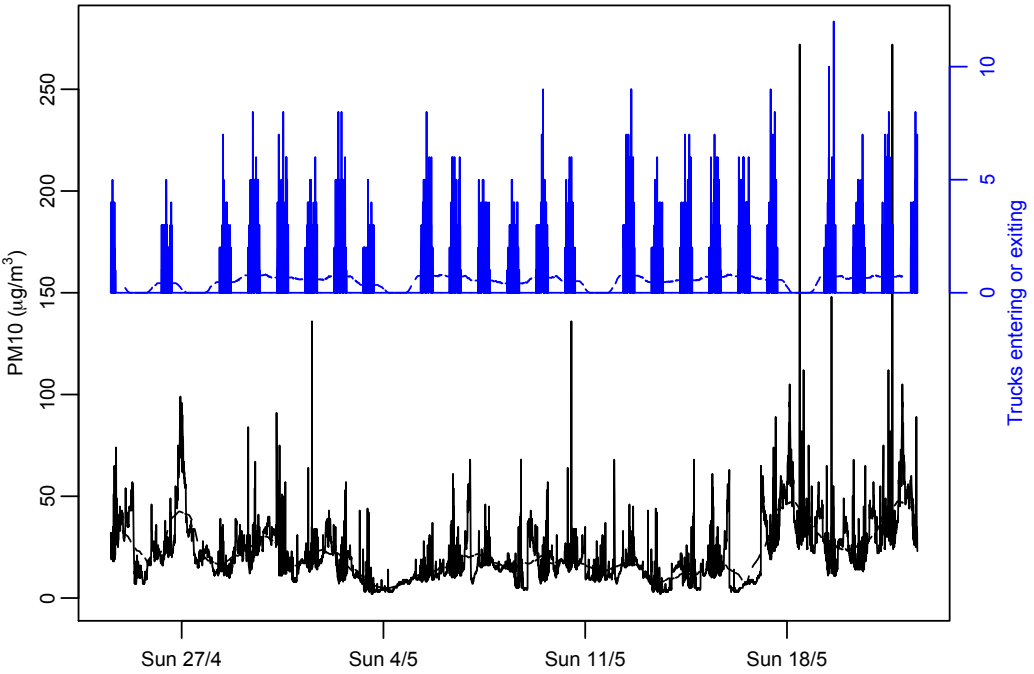

instrument failure. As we see below, the data that was collected during this period does nonetheless exhibit some expected trends that are absent at other times in 2014.

Figure 4 shows the aerosol data recorded without interruption in late April and the first part of July of 2014. No daily or weekly periodicity is apparent. Multi-day trends as shown by the daily moving average also appear to be sporadic. Conversely, the truck arrival and departure data plotted on the same figure indicate daytime worksite activity that one might expect to generate

Figure 5: Comparing hourly means, medians, and quartiles for aerosol concentration differences from the daily moving average: April/May 2014. Blue circles indicate mean values, means and quartiles are shown by the common 'box and whisker' arrangement.

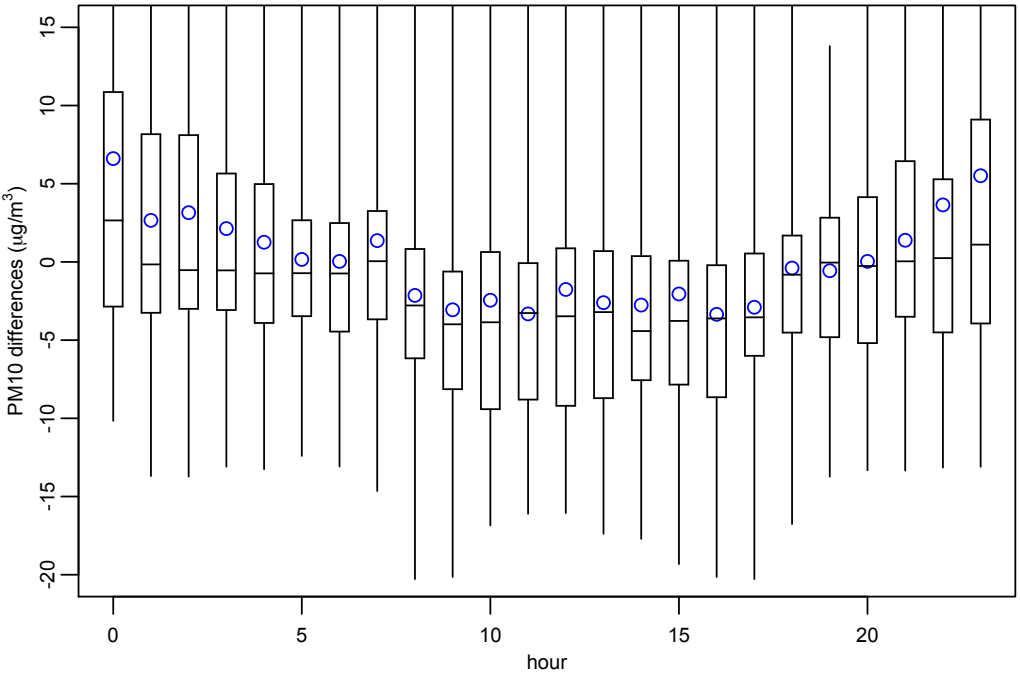

dust, typically from Monday to Saturday each week. The daily variation in aerosol concentration was investigated further by first subtracting the 24 hour moving average concentration from the raw data, and then examining data from each hour of the day in isolation. Figure 5 shows the resulting variation in the hourly means, medians and quartiles. Dust concentrations at night appear to be a little higher than those during the day: a counterintuitive result given that daytime plant operations are expected to generate dust. However, the trend is somewhat similar to the PM2.5 data taken from offsite reporting stations shown in Figure 1. It is common for the data associated with each

Figure 6: Truck traffic displayed above aerosol data of a different character recorded in October and November 2014. The number of trucks entering or exiting the worksite during five minute intervals are plotted in blue. Dashed lines show 24 hour moving averages.

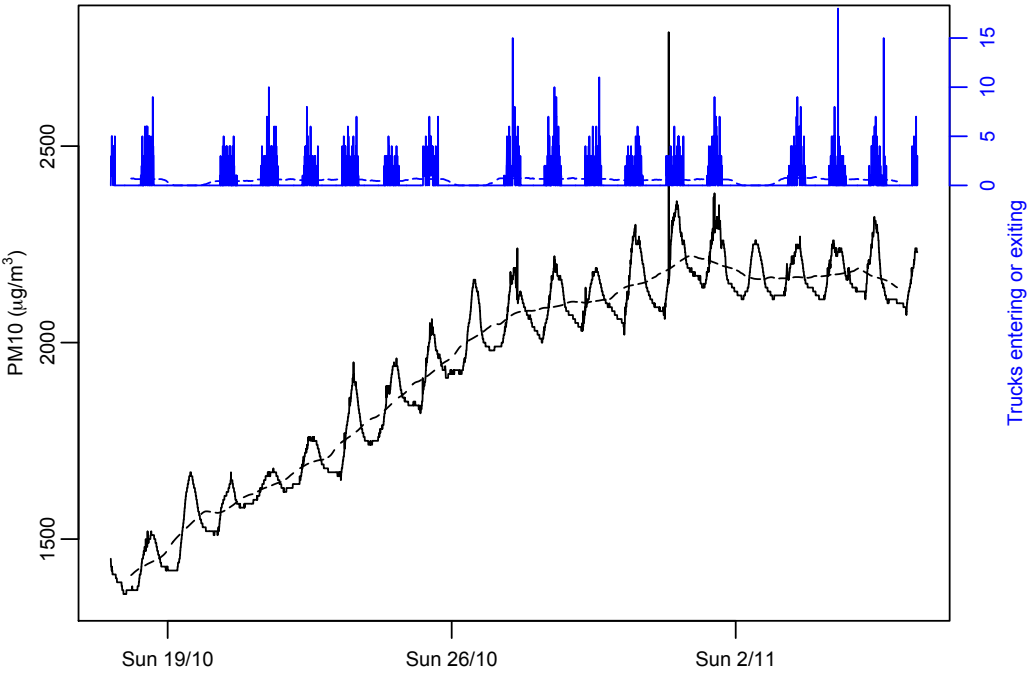

hour to exhibit a long 'tail' made up of concentration differences beyond the displayed range of Figure 5. The typical maximum concentration difference was near 50 µg/m^3, with two larger maxima near 230 µg/m^3 observed for hours 10 and 15. The skewed nature of the distribution of several hours' data is reflected in the difference between the means and medians shown.

The device interruptions that occur near the 1st of November 2014 in Figure 3 are insignificant, allowing us to investigate the entire date range of unusually high concentration values of Figure 3 in a similar manner to that shown above

Figure 7: Comparing hourly means, medians, and quartiles for aerosol concentration differences from the daily moving average: October/November 2014. Blue circles indicate mean values, medians and quartiles are shown by the common 'box and whisker' arrangement.

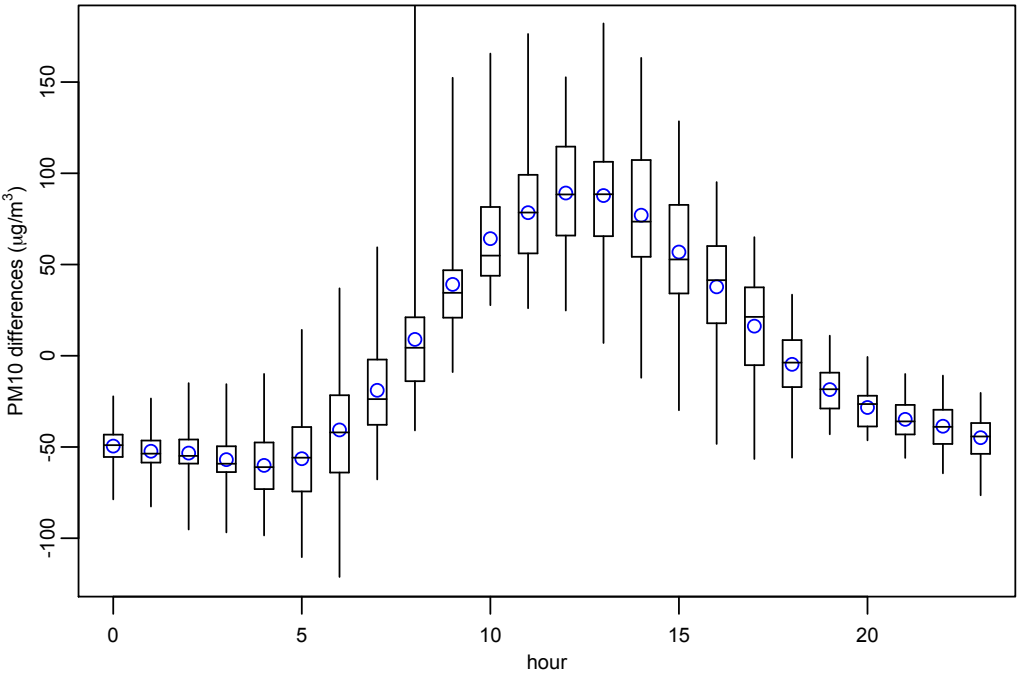

for the uninterrupted data of April and May. Figure 6 shows this data as well as the number of truck arrivals and departures during five minute intervals. In stark contrast to Figure 4, clear daily periodicity is now apparent, in addition to an extended multi-day trend in the daily average. However, whereas truck activity drops to zero on Sundays, there is no obvious corresponding decrease in the recorded aerosol concentrations on Sundays.

Figure 7 shows hourly variation after the daily moving average has been subtracted. This verifies a clear daily trend in aerosol concentrations with a peak

Figure 8: Truck traffic displayed above recent aerosol data recorded in June and July 2020. The number of trucks entering or exiting the worksite during five minute intervals are plotted in blue. Dashed lines show 24 hour moving averages.

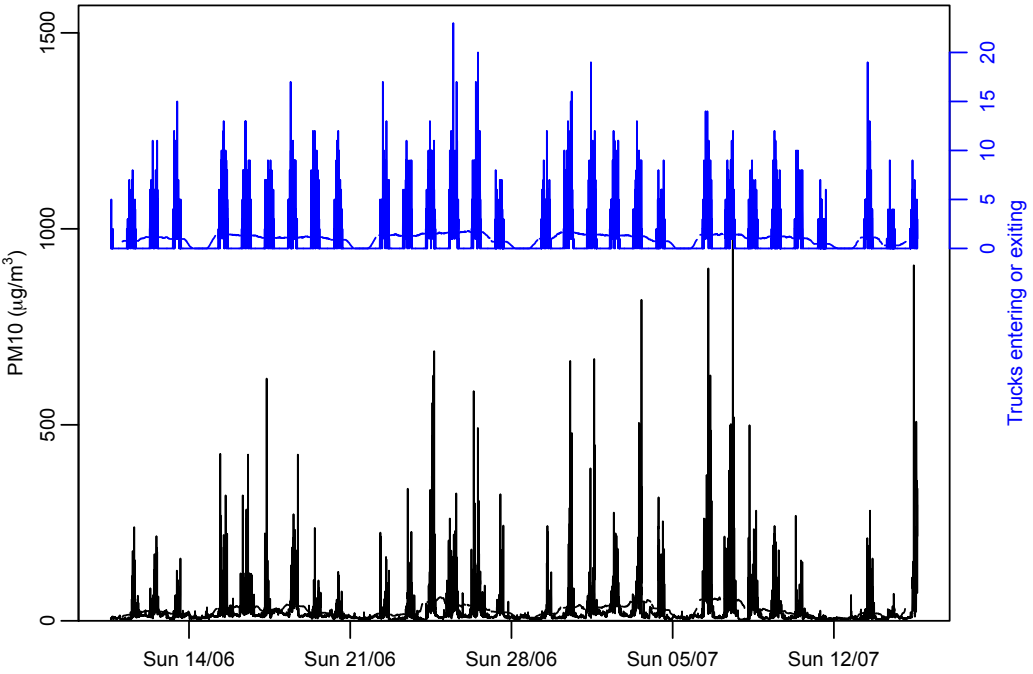

in the early afternoon. The distribution of each hour's data is approximately symmetric, without the long tails of Figure 5.

We compared the 2014 datasets above with more recent 2020 onsite data recorded using a Thompson Environmental Systems Dust Master Pro 7000 device. Similar to the Dust Trak device used in 2014, scattered laser light is used to calculate particle size distributions. The Dust Master Pro is also capable of conducting gravimetric analysis to validate the optical calculations. This is especially relevant given the unique nature of the dust generated at

Figure 9: Truck traffic displayed above aerosol data recorded on Tuesday the 16th of June 2020. The number of trucks entering or exiting the worksite during five minute intervals are plotted in blue. Dashed lines show 24 hour moving averages.

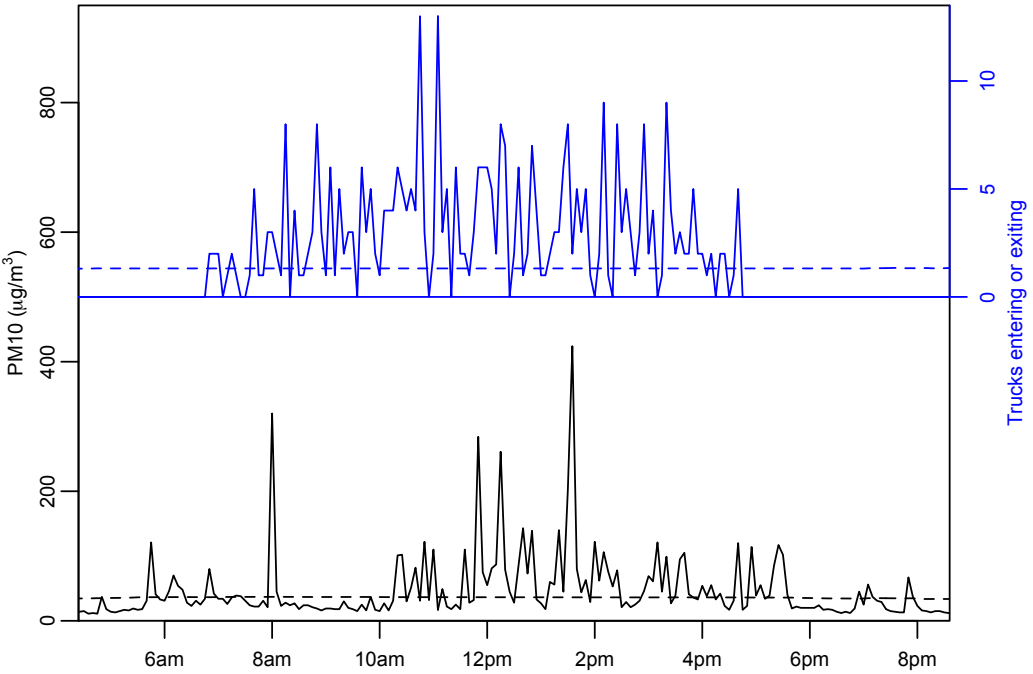

the Concrush site. The 2020 aerosol data includes a breakdown of PM2.5, PM10, and total particulate matter. The daily and weekly trends in all three recorded particulate matter types are very similar, so we investigate just the PM10 readings for consistency with the 2014 data.

Figure 8 shows an overview of the 2020 data, the qualitative features of which are different from both of the 2014 time periods considered. Unlike the data of October/November 2014, aerosol levels return to near zero each evening, and do not remain at very elevated levels. Here the recorded aerosol

Figure 10: Comparing hourly means, medians, and quartiles for aerosol concentration differences from the daily moving average: June/July 2020. Blue circles indicate mean values, medians and quartiles are shown the common 'box and whisker' arrangement.

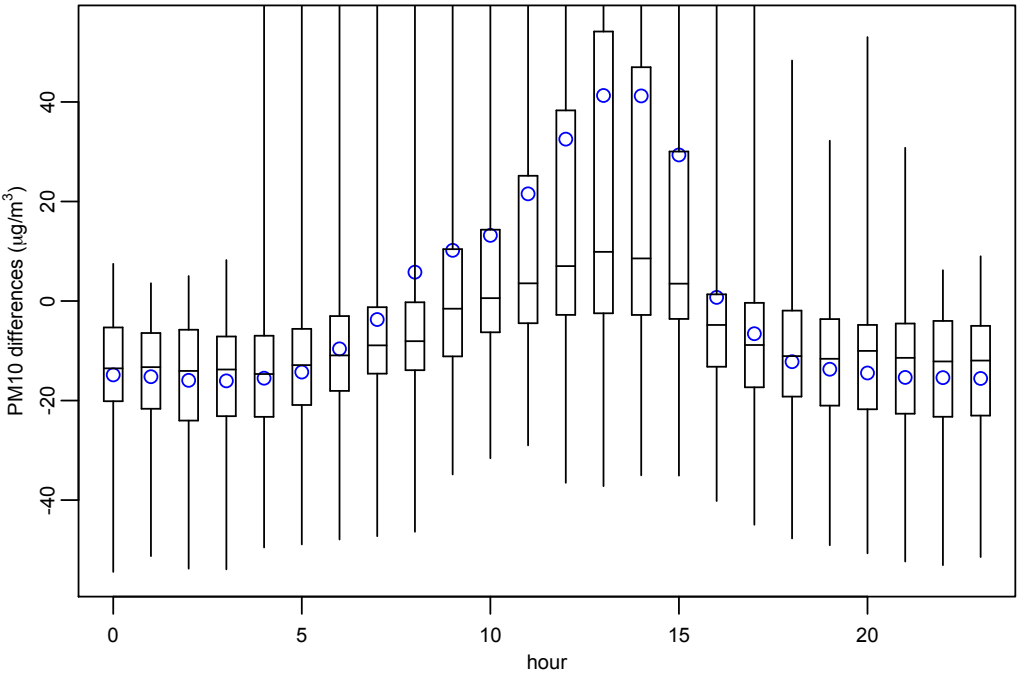

data is qualitatively similar to the truck activity frequencies shown in the same plot, with clear daytime peaks from Monday to Saturday, and low activity on Sundays. This is the natural expectation if dust generated onsite is contributing to the recorded PM10 concentrations.

Figure 9 shows a close-up view of aerosol and truck traffic data for Tuesday the 16th of June 2020. Despite PM10 aerosol levels and truck traffic both being high during workdays and low at nights, clear correlations between the two at small time-scales are not apparent by inspection in Figure 9, or for

other individual days considered.

Figure 10 is comparable to Figures 5 and 7, and illustrates the variation in hourly data after subtraction of the daily moving average. For consistency with earlier figures, no accommodation has been made for the weekly trend apparent in Figure 8. A clear peak in aerosol concentration during the early afternoon is observed, with data sets for peak hours exhibiting long tails. Datasets for night-time hours are relatively symmetric by comparison. The early afternoon PM10 aerosol peak observed is quite distinct from the two peaks during the morning and late afternoon shown in the bottom right panel of Figure 2. This qualitative difference between distinct locations could be due to several unknown factors. It is possible that the Wallsend data is heavily influenced by peak vehicle traffic flows, whereas the PM10 readings taken within the relatively small Concrush site are largely determined by local operations.

The relationship between truck traffic and aerosol concentration is further investigated in Figure 11. For each hour, statistics for aerosol concentrations that were taken during times of low, medium or high truck traffic are shown. For the daytime hours selected (those with sufficient truck traffic) there appears to be a clear trend whereby aerosol concentrations increase with truck traffic. Here asterisks placed next to the mean PM10 value for high truck traffic indicate that the mean is significantly different from the mean PM10 value for low truck traffic, for the same hour. This is the case for six of the eight hours considered. The skewed nature of the PM10 concentration distributions contribute to the low and high truck traffic means failing to be significantly different at 1 pm. Considering the logarithm of PM10 concentrations rather than the concentrations themselves produces relatively symmetric distributions with means and medians in close proximity. The mean values of log-PM10 concentrations for low and high truck traffic are significantly different from one another at $p = 0.01$ for hours 9 am to 3 pm inclusive.

We also investigate PM10 readings several minutes after different levels of truck traffic, or several minutes before different levels of truck traffic. Preliminary

Figure 11: Aerosol concentrations for low medium and high truck traffic: June/July 2020. Each hour has three datasets associated with it: the first is for zero or one truck passings, the second for two, three, or four truck passings, and the third for five or more truck passings. Blue circles indicate mean values, medians and quartiles are shown the common 'box and whisker' arrangement. An asterisk has been added next to the mean for four or more truck passings when this mean is shown to be significantly different at $p = 0.01$ from the mean for zero or one truck passings, according to an unequal variances t-test.

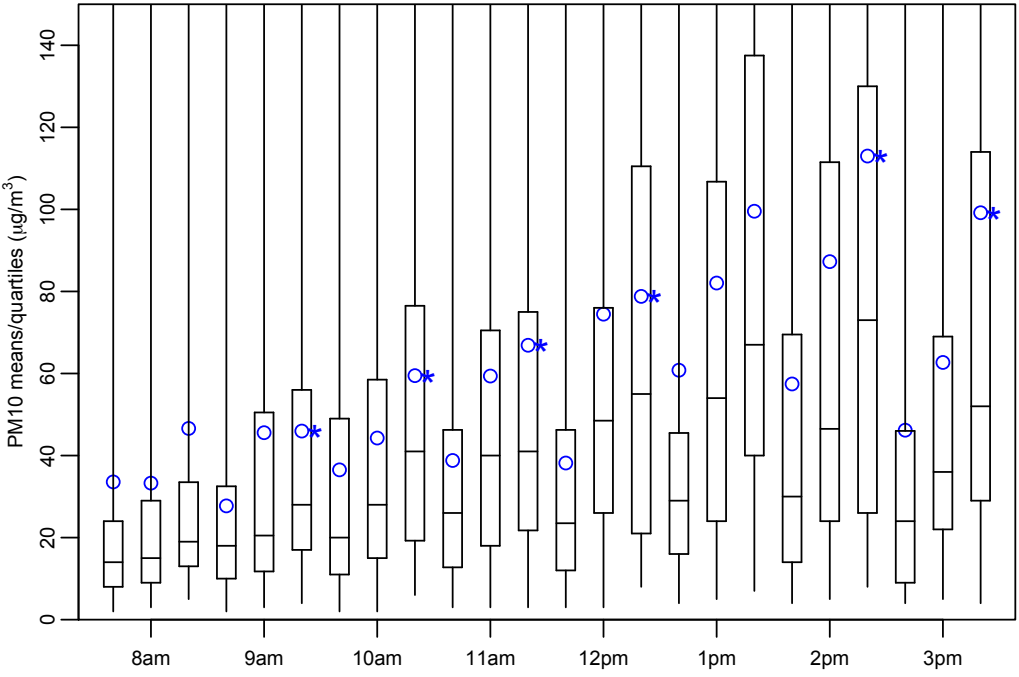

Figure 12: Wind data displayed above aerosol data recorded on Friday the 3rd of July 2020. Wind direction in degrees, and wind speed (m/s) are plotted in purple and blue respectively.

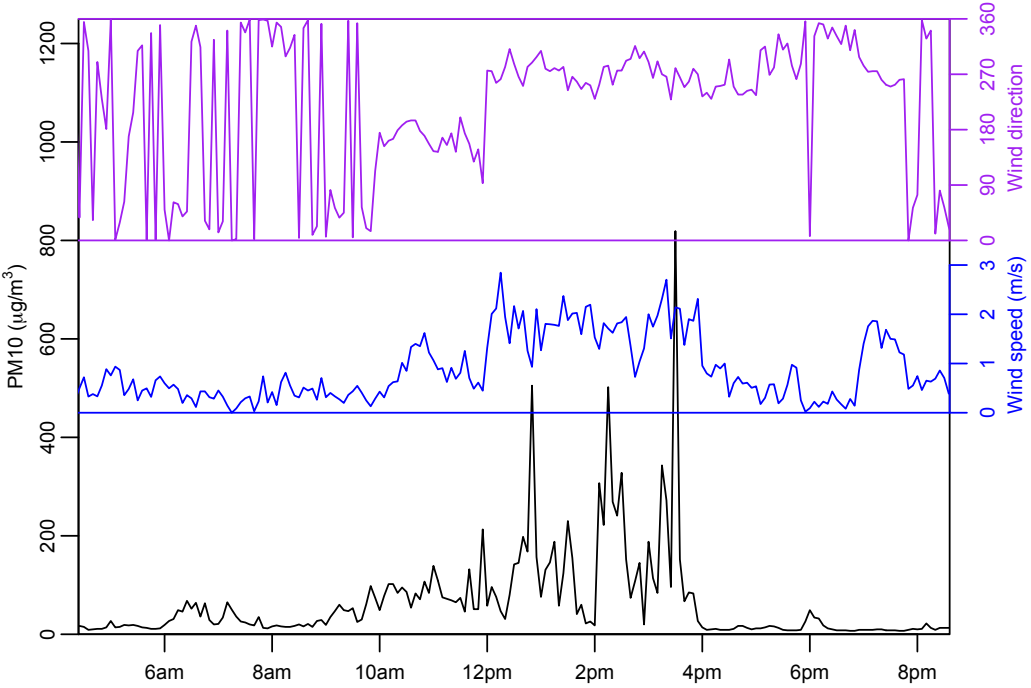

investigation along these lines indicates that dust can be significantly higher both before and after high truck traffic events. However, the correlations are not as extensive as those of Figure 11. The reason for these preemptive, or delayed dust levels may be related to whether trucks are carrying incoming or outgoing loads, the type of load material, and incomplete or inaccurate truck traffic data, none of which are considered in the present analysis.

Another feasible effect is that dust levels could be related to wind strength or wind direction, which is also recorded by the 2020 Dustmaster Pro device. Figure 12 shows PM10 data for the 3rd of July as well as wind direction and

speed data recorded concurrently. Similar analysis to that of Figure 11 has been conducted for wind speed and wind direction in isolation, but no clear correlations were observed.

A more detailed future investigation may seek to predict aerosol concentrations based on particular types of truck traffic, wind strength and direction, the nature of daytime plant operations, and additional factors. The clear qualitative differences between the data of the three time periods explored above imply unknown factors that have significant effects on collected data, and illustrate the need for consistent methods of continuous aerosol measurement made over extended periods of time.

4 Modelling the airborne transport of dust—analytical approach

To describe the transport of fugitive dust particles, the group turned to mathematical models. We considered a wide range of approaches ranging from applying a simple advection-dispersion equation, to adapting more complex models from other applications. Namely, we considered adapted versions of a saltation model and a bushfire ember plume model. In Section 5 we explore a numerical model of individual particles.

The advection-dispersion model contained two basic phenomena: the advection of dust particles by background wind, and the dispersal of dust particles. For a first pass, we assume that a certain amount of dust is released in a narrow vertical column, and then assume that the wind and dispersal only act horizontally. This allows us to obtain an exact 2D solution by taking advantage of some properties within our model. This solution describes the dust concentration at any given point at any given time in the surrounding area.

We also took into account the settling and deposition of dust particles onto the ground surface. The vertical settling of small dust particles can be set

by the Stokes velocity, which describes a linear loss of mass over time. The model accommodates classes of different particle size, and as a result, larger particles fall swiftly, whereas small particles fall slowly and may travel far with the help of wind. Computer based simulations were also implemented and verified against the exact results. This allows us to extend the simple model with additional physical phenomena and obtain a numerical solution. Non-point sources, wind shear and particle interference would all require numerical treatment.

We considered a saltation model to describe the motion of particles as they "skip" along the ground. Such models are traditionally used to described the erosion and evolution of dunes and other sand patterns on desert landscapes. This model gives us insight into the behaviour of different sized particles, how they interact with the ground, and how they are influenced by wind and turbulence.

We also investigated the utility of an ember plume model (Roberts, Sharples, and Rawlinson 2017; Roberts, Rawlinson, and Wang 2021) to describe the aggregation of dust from dispersion sources over a large geographic area. This approach demonstrated that dust collected in the Concrush gauges could potentially have been generated off site. However, further data is required to determine the likelihood of this scenario. To use this approach, we would characterise the geography surrounding Concrush to determine the source of both background and emitted dust levels. However, realistically we need more data.

The advection-dispersion model describing the transport of dust through the air provided the best way forward of these approaches, and is explored here further. We begin with a very simple model, and then slowly add more functionality and details.

4.1 Dispersion

Typically, the dispersion of dust is modelled by the advection-diffusion equation (Eltayeb and Hassan 2000)

$$\frac{\partial c}{\partial t} + \mathbf{u} \cdot \nabla c = \boldsymbol{\nabla} \cdot (D \cdot \nabla c), \tag{1}$$

where $\mathbf{x} = (x, y, z)$, $\boldsymbol{\nabla} = \left(\frac{\partial}{\partial x}, \frac{\partial}{\partial y}, \frac{\partial}{\partial z}\right)$, and where c is the concentration (typically $\mathrm{kg\,m^{-3}}$), t is time and $\mathbf{u} = (u, v, w)$ is the background air movement. For simplicity, we take $\mathbf{u}$ to be the wind vector and assume it is constant everywhere. The parameter D is the dispersion (diffusion) coefficient. In this case, it does not describe molecular diffusion, but describes the seemingly random movement of dust particles under the influence of turbulent eddies. We use the term "dispersion" to refer to both the parameter D and the PDE (1) over "diffusion" to emphasise this distinction. A stronger wind may increase the value of D. Some consider D to be dependent on the height of the particle, due to the decreasing presence of wind close to the ground, using logarithmic or linear functions of height (Eltayeb and Hassan 2000). For simplicity of the transport model, we assume a constant value for D, which captures the macro-scale behaviour of dust.

To begin with, we only model the horizontal transport of dust. We discuss the vertical transport and settling behaviour in Section 4.2. For mathematical convenience, let us consider the instantaneous generation of a cloud of dust with total mass, M. In line with our horizontal transport model, let us assume that the entire initial cloud is generated in an infinitesimally thin column of height H.

Let us first define a moving coordinate system to adjust for wind. That is, let $\mathbf{x}' = \mathbf{x} - \mathbf{u}t$. The dispersion equation (1) then becomes

$$\frac{\partial c}{\partial t} = \boldsymbol{\nabla}' \cdot (D \cdot \nabla' c), \tag{2}$$

where $\boldsymbol{\nabla}' = \left(\frac{\partial}{\partial x'}, \frac{\partial}{\partial y'}\right)$. The advection term has been completely removed in this moving frame of reference. Then, we reformulate the dispersion equation

in cylindrical coordinates to

$$\frac{\partial c}{\partial t} = \frac{D}{r}\frac{\partial}{\partial r}\left(r\frac{\partial c}{\partial r}\right), \tag{3}$$

where $r = \sqrt{(x')^2 + (y')^2}$. The θ coordinate is absent from the dispersion equation (3) due to the cylindrical symmetry of the initial cloud. The PDE (3) has a known similarity solution

$$c(r,t) = \frac{M}{4\pi DHt}\exp\left(\frac{-r^2}{4Dt}\right). \tag{4}$$

The pre-factor of the solution (4) is chosen so that the mass of dust is conserved for all time. That is,

$$M = \int_0^H \int_0^{2\pi} \int_0^{\infty} c(r,t) r \, dr \, d\theta \, dz. \tag{5}$$

Transforming back into stationery Cartesian coordinates, the solution is

$$c(x,y,t) = \frac{M}{4\pi DHt}\exp\left[\frac{-(x-ut)^2-(y-vt)^2}{4Dt}\right]. \tag{6}$$

For illustration, we plot three sets of solutions on the x-plane in Figure 13. Each figure shows the concentration profile evolving in time, for three example wind speeds. For no wind (Figure 13a), the profile simply broadens over time, and dust is only transported by dispersion. For a small amount of wind (Figure 13b), the center of the diffusing profile moves. A small amount of dust travels upwind, while most is transported downstream. For a large wind (Figure 13c), the dust is almost entirely transported downwind.

It may appear that the profiles in Figure 13 are losing mass. Mass is conserved overall, but there is mass loss in the x-plane over time due to the dispersion in the y-direction.

Figure 13: Three sets of solutions for the concentration of dust transported by dispersion and wind advection. Example parameters are $D = M = H = 1$, with varying wind speeds in the x-direction. The concentration profile broadens as time progress from $t = 0.5$(blue), 1(orange), to 2(green).

(a) For wind speed, $u = 0$.

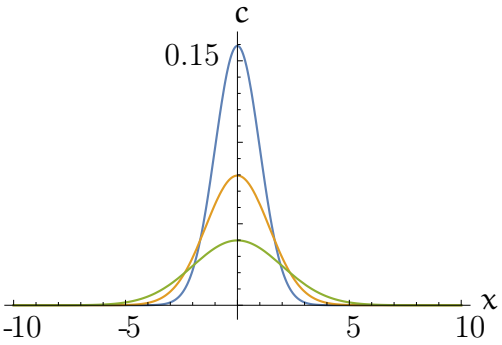

(b) For wind speed, $u = 1$.

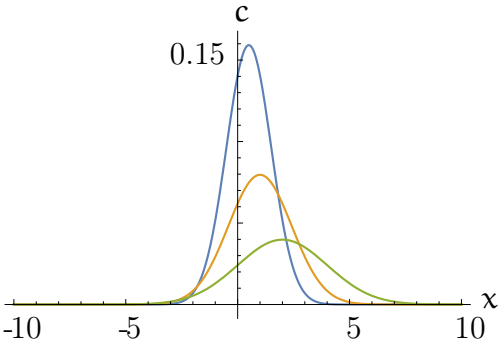

(c) For wind speed $u = 5$.

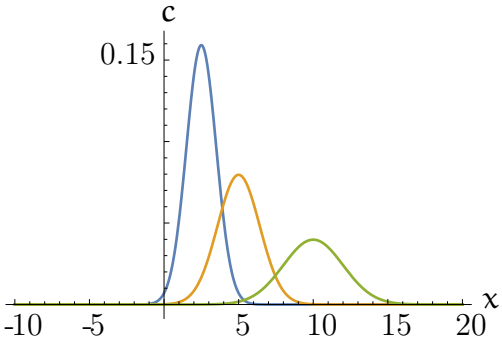

4.2 Settling and deposition of particles

One of the the important questions we need to address is: how far does the dust travel? The simple dispersion model above does not address this; the dust particles disperse and advect horizontally. We need to take into consideration the vertical settling of dust.

One simple way to model dust settling is to consider the Stokes settling velocity (Stokes 1851). The Stokes settling velocity is valid in the viscous flow regime, and we assume that the particles swiftly reach the terminal velocity.

Table 1: Table of physical parameters

Parameter	Description	Value	Units
ρ_s	Density of solid	2.20×10^3	$\mathrm{kg\,m^{-3}}$
ρ_a	Density of air	1.225	$\mathrm{kg\,m^{-3}}$
g	Gravitational acceleration	9.8	$\mathrm{m\,s^{-2}}$
μ	Dynamic viscosity of air	18.0×10^{-6}	$\mathrm{N\,s\,m^{-2}}$
ν	Kinematic viscosity of air	14.9×10^{-6}	$\mathrm{m^2\ s^{-1}}$

The terminal velocity of spherical individual particles is

$$w = \frac{1}{18}\frac{\Delta\rho g d^2}{\mu}, \tag{7}$$

where g is gravitational acceleration, d is the particle diameter, μ is the dynamic viscosity of air, and $\Delta\rho$ is the density difference between the solid and air. Realistically the difference is so large compared to the density of air that we set $\Delta\rho = \rho_s - \rho_a \approx \rho_s$, where ρ_s and ρ_a are the density of the solid and air, respectively.

Large solid particles fall quite fast, and Stokes may not apply here. Using the physical parameters listed in Section 4.2, we seek to find the particle size where Stokes settling may no longer be appropriate.

The Stokes velocity applies if the Reynolds number is less than approximately one. The Reynolds number is defined by

$$\mathrm{Re} = \frac{wL}{\nu}, \tag{8}$$

where ν is the kinematic viscosity, and L is the characteristic length, which we take to be the particle diameter. Setting $\mathrm{Re} = 1$ and presuming a Stokes velocity, we solve equations (7) and (8) for the particle diameter. We find that the "critical" diameter (where $\mathrm{Re} = 1$) is about 73.9 µm. The Stokes velocity applies for particles with diameters much smaller than this value, but

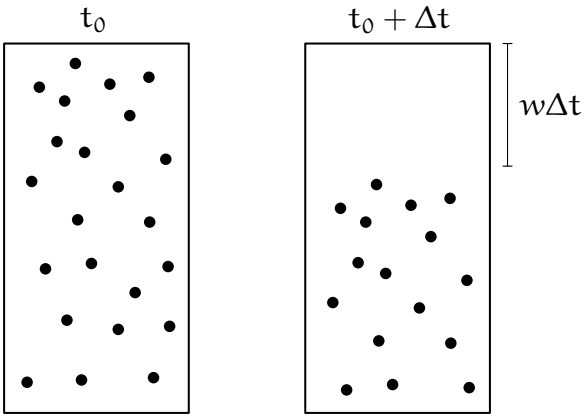

Figure 14: A conceptual figure showing the linear settling of dust particles.

it becomes less valid as the particle size approaches this "critical" value. Since the emitted dust has particle sizes below about 50 µm, the Stokes velocity seems appropriate, at least to a self-consistency check.

The vertical settling behaviour of particles can thus be considered as simple linear motion. For a high density of solid particles or a high fluid viscosity, they may interfere with each other, leading to nonlinear behaviour (Richardson and Zaki 1955), but that is unlikely in this application. Due to its linearity, we incorporate the vertical settling behaviour into our 2D solution to make it pseudo-3D.

Figure 14 shows a conceptual diagram of suspended solid particles, slowly sinking under the effects of gravity. A proportion of the solid mass is lost over time. All suspended mass is lost when the highest dust particles in the initial column are deposited on the ground, which occurs after $t = H/w$, where H is the height of the initial column.

The linear loss of mass over time can be incorporated into our solution (6) to give

$$c(x, y, t) = \frac{M}{4\pi DHt} \exp\left[\frac{-(x - ut)^2 - (y - vt)^2}{4Dt}\right]\left(1 - \frac{wt}{H}\right). \qquad (9)$$

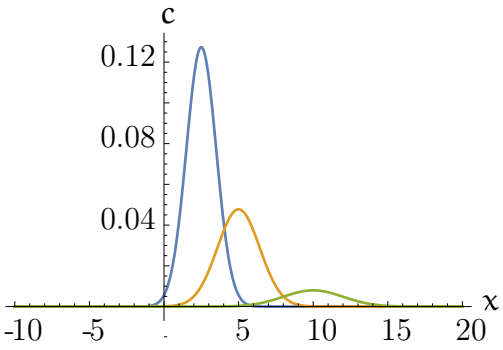

Figure 15: A solution profile for $t = 0.5, 1, 2$ seconds (respectively blue, orange, green). As time progresses the concentration profile moves due to wind, broadens due to dispersion, and loses mass to particle deposition.

Figure 15 shows the concentration profile (9) as time evolves. We use particles with a settling speed of $w = 0.4\,\mathrm{m\,s^{-1}}$. The particle settling speed (7) is a function of both particle size and particle density. For the parameter values in Section 4.2 this equates to a particle diameter $\approx 78\,\mu\mathrm{m}$. All other parameters are analogous to Figure 13c for comparability. We see that for this illustrative example, most particle mass is deposited within 15 m downstream of the source.

The aim of this simple model is to give us an idea about how far the dust produced by Concrush travels. Parameters can be chosen by physical values in the literature, or tuned by the available onsite data.

If we find a more complicated model is required, then there are avenues in the literature (e.g., Eltayeb and Hassan (2000) used a CFD modelling approach, and Guo et al. (2020) included a linearly varying wind speed with height and considers both point and line sources).

4.3 Transport of polydisperse dust

Dust particles generated by Concrush operations are not all the same size. That is, they are not monodisperse. What is observed, is a polydisperse distribution of dust particles, spanning many sizes. The settling behaviour is dependent on particle size; large particles fall very fast. The dispersion

parameter may also be size-dependent. The broad particle size distribution can be accommodated by the above simple model. Assuming there is no interactivity between particles, we solve the above transport equation for multiple different particle sizes. The particle size distribution can be discretised into an arbitrary number of classes, each with its own governing equation and solution. For example, a particle in class k would have a diameter of d_k.

The solution for each class, k, is

$$c_k(x,y,t) = \frac{M_k}{4\pi D_k H t} \exp\left[\frac{-(x-ut)^2-(y-vt)^2}{4D_k t}\right]\left(1-\frac{w_k t}{H}\right). \quad (10)$$

The mass of dust within each class is M_k, and the total dust mass is $M = \sum_k^N M_k$, where N is the number of classes. The settling velocity of each class is

$$w_k = \frac{1}{18}\frac{\Delta\rho g d_k^2}{\mu}. \quad (11)$$

As an example, consider a three-class model. Figure 16 shows the evolution of the dust cloud for three particle sizes over time. The initial mass of each particle class size released into the dust cloud is the same. We see that the heavy particles quickly lose mass to deposition and so do not travel far. The smallest particles have no appreciable deposition at all, and may remain suspended in the air, travelling a large distance. The parameters are taken from Section 4.2, with $H = 2\,\mathrm{m}$, and $u = 2.87\,\mathrm{m\,s^{-1}}$. Table 2 shows the parameters for each of the three particle classes.

4.4 Example calculation

The solution (10) is quite versatile. One use is to determine the concentration of pollutant dust at a particular location. For example, let us release 10 g of PM2.5 dust in a 2 m high column at a particular location in 10 km/h wind. What will the concentration of dust be 1 km downwind? We use the same physical parameters as in Figure 16, except for the dispersion coefficient,

Table 2: Parameter values used to produce Figure 16. The values of the dispersion coefficient, D, are purely illustrative.

k	d_k (μm)	M_k (kg)	D_k ($m^2\ s^{-1}$)
1	5	5	0.1
2	80	5	1
3	200	5	10

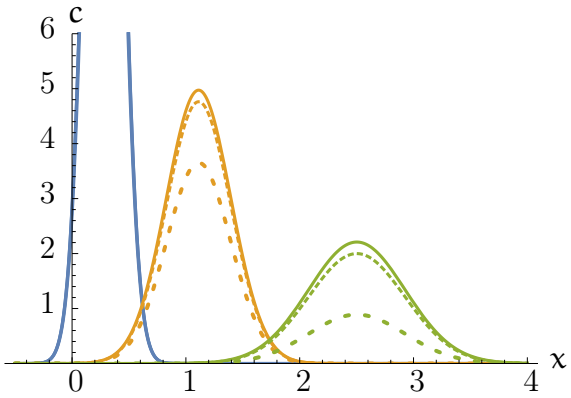

Figure 16: The evolution of the concentration profiles over time (left to right, $t = 0.05$, $t = 0.2$ and $t = 0.45$ s) for three different particle classes: The particles have diameter 5 μm (solid), 80 μm (dashed), and 200 μm (dotted).

where we try to use a realistic value. It turns out to be very difficult to do, as reported values vary wildly. For example, Baughman, Gadgil, and Nazaroff (1994) report a value of $D = 1.83 \times 10^{-3}\ m^2\ s^{-1}$ for indoor dispersion of pollutants. Outdoor dispersion should be a bit higher than this due to wind eddies, but we take this as a representative lower bound.

Using these values we calculate that 360 seconds after the initial release of dust, our sensing location will experience its maximum pollutant concentration of $3.86\ mg\ m^{-3}$. If the wind increases to 30 km/h, then the maximum concentration is $9.35\ mg\ m^{-3}$ and occurs sooner at $t = 180$ s. The concentration profiles over time are shown in Figure 17. In the stronger wind, the dust cloud reaches the sensor sooner, and has not had as much time to disperse, leading to a higher and narrower concentration profile.

Figure 17: The concentration ($\mathrm{mg\,m^{-3}}$) profile over time for a sensor 1 km downwind of a 10 g source of dust.

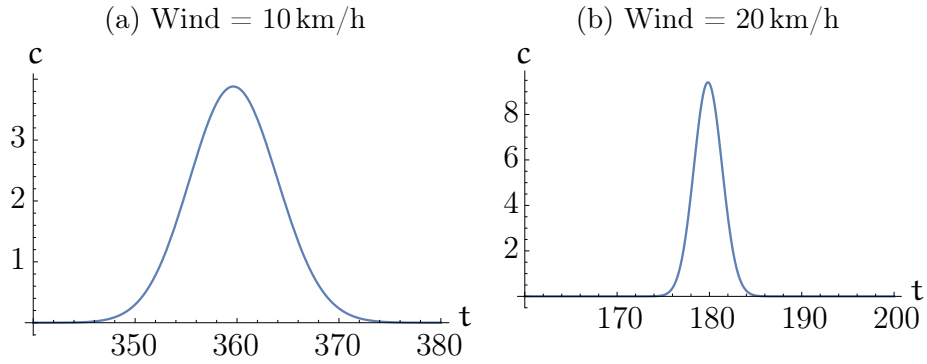

While we attempted to use a "realistic" value for the dispersion parameter, there is a lot of uncertainty about the appropriate value to use. The ideal situation would be to carry out some dust plume experiments on site in various wind conditions, and use a downwind sensor as in the example. The dispersion parameter obtained by such an experiment would be ideal to input into our model for predictive power.

5 Numerical model of single particles

The model described in the previous Section 4 allows us to calculate almost instantaneously the dust concentration following the release of particles at a known location and height everywhere and at any time. However, finding the right parameters for this type of model can be very challenging. In this section, the dust movement is studied by simulating individual particles. This approach trades computational cost for improved model assumptions. The advantage of this method is that the parameters are easier to estimate, and we can relax some assumptions necessary for the analytical model in Section 4. The disadvantage is that resolving the differential equations

multiple times over for each particle makes it computationally demanding. The computational cost effectively limits our exploration to low wind speeds. Under strong wind conditions the particles generally travel large distances from their release site, as shown by the model in Section 4, which is very costly to simulate. This model is therefore best suited for exploring dust movement under lower wind conditions.

The equations described by Kok and Renno (2009) allow the numerical calculation of the motion of single particles. According to their study, the "Staffman force" and "Magnus force" are the forces that have the least effect on the particle motion. These forces are ignored in this MISG study in order to simplify the equations and reduce the computational cost.

For this MISG problem, we consider the motion of cement particles. The particles' motion depends only on their weight and the drag force. Like Kok and Renno (2009), we consider that the cement particles do not have a perfect spherical shape because they have irregularities at their surface, which leads to a higher drag, which is a more realistic assumption than that used in Section 4. The equation of motion is

$$\begin{bmatrix} a_x \\ a_y \\ a_z \end{bmatrix} = -\frac{3}{4}\frac{\rho_a}{\rho_p}\frac{C_d}{d_p} v_R \left(\begin{bmatrix} v_x \\ v_y \\ v_z \end{bmatrix} - \begin{bmatrix} U_x \\ U_y \\ U_z \end{bmatrix} \right) - \begin{bmatrix} 0 \\ 0 \\ g \end{bmatrix} \tag{12}$$

with a is the acceleration, ρ_a is the air density, ρ_p is the particle density, d_p is the particle diameter, C_d is the drag coefficient, v_R is relative particle speed, v is the particle speed, U is the wind speed, and g is the gravity.

The wind speed U is split into a mean component $\bar{U}$ and a random component U'. We assume a horizontal flow in the x-direction, which means that $\bar{U}_y$ and $\bar{U}_z$ are zero. Therefore, the wind speed is

$$\begin{bmatrix} U_x \\ U_y \\ U_z \end{bmatrix} = \begin{bmatrix} \bar{U}_x \\ 0 \\ 0 \end{bmatrix} - \begin{bmatrix} U'_x \\ U'_y \\ U'_z \end{bmatrix}, \tag{13}$$

where $\bar{U}_x$ is zero at the ground level ($z = 0$) and increases logarithmically with the height z. The random components of the wind are based on the standard deviations of the wind speed in a homogeneous and isotropic turbulence, which depends on z and $\partial \bar{U}_x / \partial z$. The particle remains a short time in the same eddy before moving to the next one. This phenomenon is reproduced by linking the random velocities separated by a short time step using a modified Lagrangian timescale. Kok and Renno (2009) gave a detailed description of the wind speed. Once the particle hits the ground, it is "captured" and can no longer move.

A height-dependent wind speed with turbulence provides for a more realistic scenario than the constant wind speed used in Section 4.

Particles of cement ($1440\,\mathrm{kg\,m^{-3}}$) were simulated starting at rest at 2 m height. We tested three diameters (5, 10, and 50 µm) and two wind conditions (2 and $3\,\mathrm{m\,s^{-1}}$ in the x-direction at a height of 2 m). The $3\,\mathrm{m\,s^{-1}}$ simulations (orange lines in Figures 18 and 19) are equivalent to the 10 km/h wind speed in Figure 17a. For these simulations we focus on smaller particle sizes, since the analytical solution in Section 4 demonstrates that larger particles settle rapidly. Fifty particles were simulated in each case.

The movements in the zx-plane of 50, 10 and 5 µm particles are shown in Figure 18. The 50 µm particles (Figure 18(a)) barely move from their point of release and fall almost vertically regardless of the wind condition, which is consistent with the results in Section 4, whereas the 10 µm particles (Figure 18(b)) and 5 µm particles (Figure 18(c)) typically travel over several meters before hitting the ground, especially when the wind speed is high. As expected, smaller particles tend to drift further away and a stronger wind increases the drift. The movement of the smallest particles is also more affected by the wind turbulence (eddies), which increases their dispersion on the ground. The particle dispersion in the x-direction (parallel to the wind direction) becomes much higher than in the y-direction (perpendicular to the wind direction) when the drift is high. This effect is represented in Figure 19, where the movement of the 5 µm particles is drawn in the xy-plane.

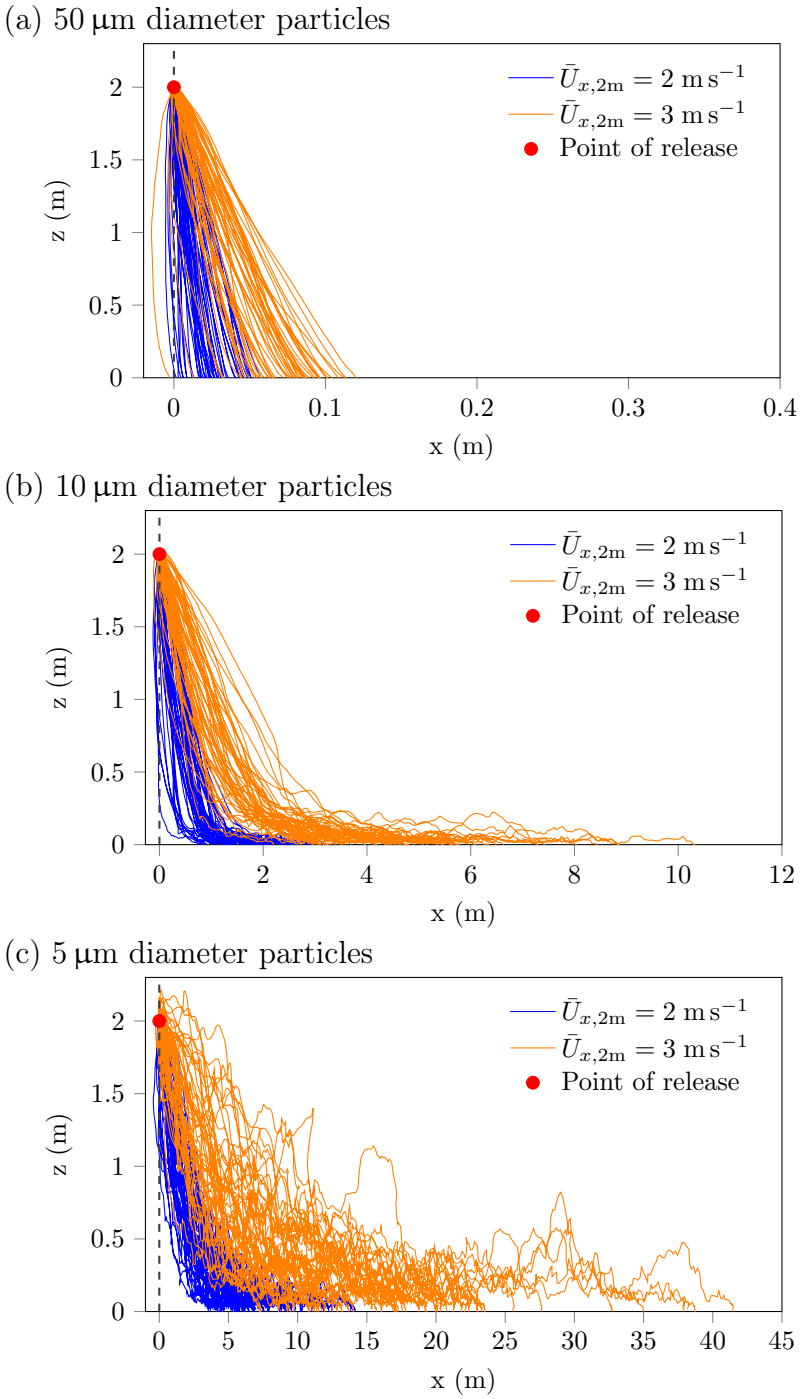

Figure 18: Side view (zx-plane) of 50 particles with a diameter of (a) 50 µm, (b) 10 µm, and (c) 5 µm released at 2 m high under two wind conditions. The 2 and 3 $m\,s^{-1}$ indicated in the legends correspond to the average wind speed at 2 m high.

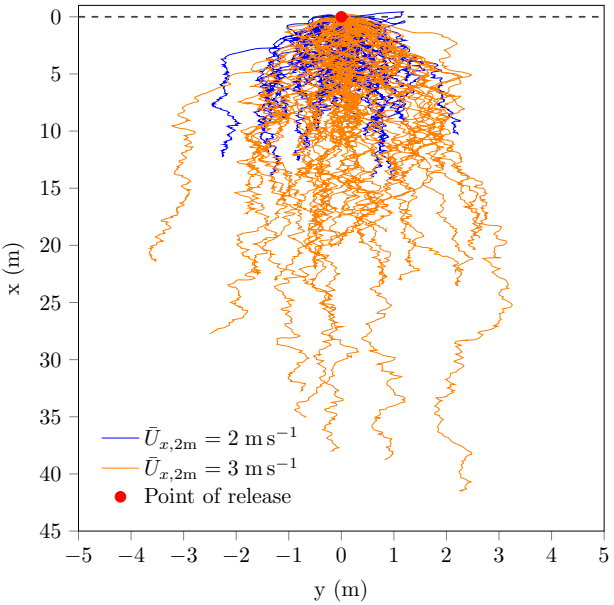

Figure 19: Top view (xy-plane) of 50 particles with a diameter of 5 µm released at 2 m high under two wind conditions. The 2 and 3 $\mathrm{m\,s^{-1}}$ indicated in the legend correspond to the average wind speed at 2 m high.

The number of simulated particles is low, so the median distance travelled in the x-direction is calculated to represent the main behaviour of the different particle sizes, thus avoiding bias due to extreme values. Figure 20 displays the median travelled distance in the x-direction for the different particle diameters under two wind conditions. Due to the computational time, we limited our particle size to 5 µm but from Figure 20, we expect particles with a diameter below 2.5 µm to travel over hundreds of meters for a strong wind.

6 Conclusion

Minimising dust generation and dispersion is a priority for Concrush, both to ensure they are compliant with EPA regulations, and for the protection of their employees and the community. However, as the regulations have been developed based on knowledge of coal industries, their appropriateness

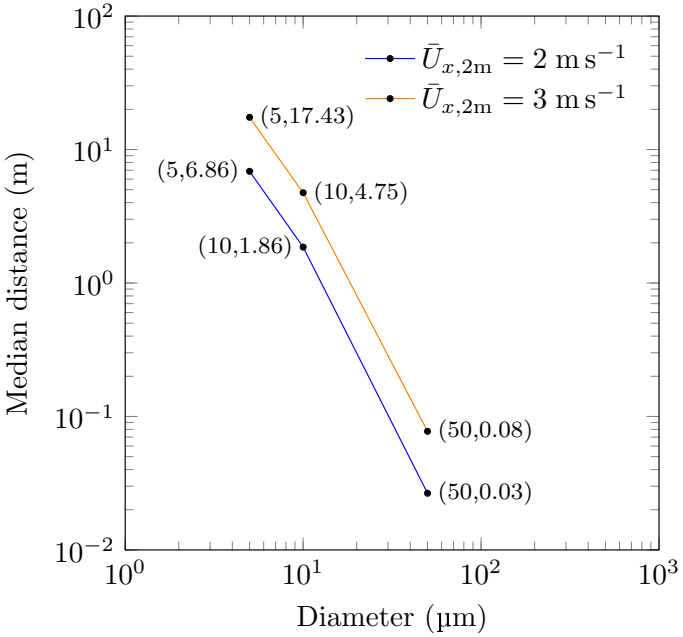

Figure 20: Median distance travelled by 50 particles with a diameter of 5, 10 and 50 µm released at 2 m high under two wind conditions. The 2 and 3 $m\,s^{-1}$ indicated in the legend correspond to the average wind speed at 2 m high.

in a concrete recycling facility requires investigation. This Mathematics-in-Industry Study Group explored three key questions about dust generation and transport: the critical process for production, origins of dust collected in the Concrush dust gauges, and potential final fate of dust generated by Concrush. To examine these questions a combination of a review of the literature, data analysis and modelling of dust transport was employed.

Our analysis showed that reducing wind speed on site provides the best opportunity to limit fugitive dust escaping the Concrush site. While Concrush already cease operations during high-wind events, stock pile placement and the use of windbreaks could further reduce fugitive dust transport. Analysis of air quality data identified an afternoon peak for dust concentrations and correlation between high truck movement and on-site dust concentrations. The advection-dispersion model illustrates that large, heavy particles rapidly drop out of the air, but small particles can be transported large distances.

This result was corroborated by the numerical simulation, which incorporated more realistic assumptions including a variable wind speed with height above the ground and non-spherical particle shapes. The simplified version of Kok and Renno (2009)'s model adapted to the motion of cement particles suggests that in order to prevent fugitive dust from polluting the environment outside the Concrush site one should

1. limit the production of particles with a diameter smaller than 10 µm, and
2. avoid creating dust in draughty conditions.

Both the data analysis and modelling did not rule out the potential of dust collected by the perimeter dust gauges to have originated offsite. Further data is required to establish the dominant sources of dust in the perimeter gauges.

This MISG challenge was in part motivated by the question of whether concrete dust behaves differently to coal dust, as regulations have been based around studies on fugitive coal dust. A critical difference between coal and concrete dust is the density of the dust particles, with concrete dust being potentially 1.5 to 2 times the density of coal dust. This means that we expect concrete dust to settle out of the airflow at a much faster rate than coal dust. Our modelling and literature review suggests that this means concrete dust is less likely to be entrained by the wind, and more likely to fall close to the release point. Further research is required to more completely test the question of whether this means the coal-focussed regulations are appropriate in a concrete recycling context or if modifications would be sensible.

Acknowledgements The moderators thank the industry representative, Kevin Thompson, for being available for the entire week. We also acknowledge the hard work and contributions of the group members: Susam Boral, J. Divahar, John Knight, Cameron Lord, Ognjen Orozovic, Björn Rüffer, Tarun Srivastava, Thien Tran-Duc, Kyle Stevens, and Jennie Trumpeta.

References

Badr, T. and Jean-Luc Harion (2007). "Effect of aggregate storage piles configuration on dust emissions". In: *Atmospheric Environment* 41.2, pp. 360–368. ISSN: 1352-2310. DOI: 10.1016/j.atmosenv.2006.07.038 (cit. on p. M5).

Baughman, A. V., A. J. Gadgil, and W. W. Nazaroff (1994). "Mixing of a point source pollutant by natural convection flow within a room". In: *Indoor Air* 4, pp. 114–122. DOI: 10.1111/j.1600-0668.1994.t01-2-00006.x (cit. on p. M29).

Chang, C.-T. et al. (2010). "Fugitive Dust Emission Source Profiles and Assessment of Selected Control Strategies for Particulate Matter at Gravel Processing Sites in Taiwan". In: *Journal of the Air & Waste Management Association* 60.10, pp. 1262–1268. ISSN: 1096-2247. DOI: 10.3155/1047-3289.60.10.1262 (cit. on p. M5).

Claiborn, C. et al. (1995). "Evaluation of PM10 emission rates from paved and unpaved roads using tracer techniques". In: *Atmospheric Environment* 29.10, pp. 1075–1089. ISSN: 1352-2310. DOI: 10.1016/1352-2310(95)00046-2 (cit. on p. M5).

Department of Planning, Industry and Environment's Data Download Facility. https://www.dpie.nsw.gov.au/air-quality/air-quality-data-services/data-download-facility. Accessed: 2020-07-10 (cit. on p. M7).

Diego, I. et al. (2009). "Simultaneous CFD evaluation of wind flow and dust emission in open storage piles". In: *Applied Mathematical Modelling* 33.7, pp. 3197–3207. ISSN: 0307-904X. DOI: 10.1016/j.apm.2008.10.037 (cit. on p. M5).

Eltayeb, I. A. and M. H. A. Hassan (2000). "Diffusion of dust particles from a point source above ground level and a line source at ground level". In: *Geophysical Journal International* 142, pp. 426–438. DOI: 10.1046/j.1365-246x.2000.00172.x (cit. on pp. M22, M27).

Ferreira, A. D. and R. J. Lambert (2011). "Numerical and wind tunnel modeling on the windbreak effectiveness to control the aeolian erosion of conical stockpiles". In: *Environmental Fluid Mechanics* 11.1, pp. 61–76. ISSN: 1573-1510. DOI: 10.1007/s10652-010-9176-x (cit. on p. M5).

Guo, L. et al. (2020). "The dust diffusion modeling and determination of optimal airflow rate for removing the dust generated during mine tunneling". In: *Building and Environment* 178, p. 106846. DOI: 10.1016/j.buildenv.2020.106846 (cit. on p. M27).

Hibberd, M. et al. (2013). *Upper Hunter Valley Particle Characterization Study: Final Report, 17 September 2013. CSIRO Marine & Atmospheric Research*. Government. NSW EPA. URL: https://www.environment.nsw.gov.au/-/media/OEH/Corporate-Site/Documents/Air/upper-hunter-valley-particle-characterization-study-final-report.pdf (cit. on p. M3).

Hibberd, M. et al. (2016). *Lower Hunter Particle Characterisation Study: Final Report. Report prepared by CSIRO, ANSTO and the NSW Office of Environment and Heritage on behalf of the NSW Environment Protection Authority, April 2016, NSW, Australia.* Government. NSW EPA. URL: https://apo.ansto.gov.au/dspace/handle/10238/9536 (cit. on p. M3).

Higginbotham, N. et al. (2010). "Environmental injustice and air pollution in coal affected communities, Hunter Valley, Australia". In: *Health & Place* 16.2, pp. 259–266. ISSN: 1353-8292. DOI: 10.1016/j.healthplace.2009.10.007 (cit. on p. M3).

Kok, J. F. and N. O. Renno (2009). "A comprehensive numerical model of steady state saltation (COMSALT)". In: *Journal of Geophysical Research: Atmospheres* 114, pp. 1–20. DOI: 10.1029/2009JD011702 (cit. on pp. M31, M32, M36).

Petavratzi, E., S. Kingman, and I. Lowndes (2005). "Particulates from mining operations: A review of sources, effects and regulations". In: *Minerals Engineering*. JKMRC International Student Conference, September 2004 18.12, pp. 1183–1199. ISSN: 0892-6875. DOI: 10.1016/j.mineng.2005.06.017 (cit. on p. M5).

Pope III, C. Arden et al. (2002). "Lung Cancer, Cardiopulmonary Mortality, and Long-term Exposure to Fine Particulate Air Pollution". In: *JAMA* 287.9, pp. 1132–1141. ISSN: 0098-7484. DOI: 10.1001/jama.287.9.1132 (cit. on p. M4).

Richardson, J. F. and W. N. Zaki (1955). "Sedimentation and fluidisation". In: *Transaction of the Institution of Chemical Engineers* 32, pp. 35–53 (cit. on p. M26).

Roberts, M. E., J. J. Sharples, and A. A. Rawlinson (Dec. 2017). "Incorporating ember attack in bushfire risk assessment: a case study of the Ginninderry region". In: *22nd International Congress on Modelling and Simulation*. Hobart, Tasmania, Australia, pp. 1–8. URL: https://www.mssanz.org.au/modsim2017/H10/roberts.pdf (cit. on p. M21).

Roberts, Melanie E., Andrew A. Rawlinson, and Ziyuan Wang (2021). "Ember risk modelling for improved wildfire risk management in the peri-urban fringes". In: *Environmental Modelling & Software* 138, p. 104956. ISSN: 1364-8152. DOI: 10.1016/j.envsoft.2020.104956 (cit. on p. M21).

Sairanen, M., M. Rinne, and O. Selonen (2017). "A review of dust emission dispersions in rock aggregate and natural stone quarries". In: *International Journal of Mining, Reclamation and Environment*. ISSN: 1748-0930. DOI: 10.1080/17480930.2016.1271385 (cit. on p. M6).

Stokes, G. G. (1851). "On the effect of the inertial friction of fluids on the motion of pendulums". In: *Transactions of the Cambridge Philosophical Society* 9, pp. 8–106 (cit. on p. M24).

Stunder, B. J. Billman and S. P. S. Arya (Feb. 1988). "Windbreak Effectiveness for Storage Pile Fugitive Dust Control: A Wind Tunnel Study". In: *JAPCA* 38.2, pp. 135–143. DOI: 10.1080/08940630.1988.10466360. (Cit. on p. M6).

Toraño, J. A. et al. (2007). "Influence of the pile shape on wind erosion CFD emission simulation". In: *Applied Mathematical Modelling* 31.11, pp. 2487–2502. ISSN: 0307-904X. DOI: 10.1016/j.apm.2006.10.012 (cit. on p. M5).

Toraño, J. et al. (2009). "Dust emission calculations in open storage piles protected by means of barriers, CFD and experimental tests". In: *Environmental Fluid Mechanics* 9.5, pp. 493–507. ISSN: 1573-1510. DOI: 10.1007/s10652-009-9136-5 (cit. on p. M5).

US EPA (1995). *Compilation of air pollutant emission factors*. 5th ed. Office of Air Quality Planning, Standards, Office of Air, and Radiation, U.S. Environmental Protection Agency Research Triangle Park, NC. URL: http://purl.access.gpo.gov/GPO/LPS25603 (cit. on p. M6).

Wark, K., C. F. Warner, D. Wayne T., et al. (1998). *Air pollution: its origin and control*. Addison-Wesley. ISBN: 0-673-99416-3 (cit. on p. M6).

Watson, John G, Judith C Chow, and Thompson G Pace (2000). "Fugitive dust emissions". In: *Air Pollution Engineering Manual Second Edition*. Ed. by Wayne T. Davis. Wiley. Chap. 4, pp. 117–135. ISBN: 9780471333333 (cit. on p. M5).

Wu, X. et al. (2020). "Evaluating the impact of long-term exposure to fine particulate matter on mortality among the elderly". In: *Science Advances* 6.29, eaba5692. ISSN: 2375-2548. DOI: 10.1126/sciadv.aba5692 (cit. on p. M4).

Xing, Y.-F. et al. (2016). "The impact of PM2.5 on the human respiratory system". In: *Journal of Thoracic Disease* 8.1, E69–E74. ISSN: 2072-1439. DOI: 10.3978/j.issn.2072-1439.2016.01.19 (cit. on p. M4).

Xuan, J. (2004). "Turbulence factors for threshold velocity and emission rate of atmospheric mineral dust". In: *Atmospheric Environment* 38.12, pp. 1777–1783. ISSN: 1352-2310. DOI: 10.1016/j.atmosenv.2003.12.030 (cit. on p. M5).

Author addresses

1. **Brendan Florio**, Department of Mathematics and Statistics, University of Western Australia & CSIRO Mineral Resources, Waterford, Western Australia
mailto:brendan.florio@uwa.edu.au

orcid:0000-0001-6015-8537

2. **Fillipe Georgiou**, School of Mathematical and Physical Sciences, University of Newcastle, Callaghan, NSW 2308, Australia.
mailto:fillipe.georgiou@uon.edu.au
orcid:0000-0003-4588-5319

3. **Olivier D. Y. Huet**, School of Mathematical Sciences, Queensland University of Technology, Brisbane, Australia
mailto:olivierdominiquey.huet@hdr.qut.edu.au
orcid:0000-0001-6057-803X

4. **Melanie E. Roberts**, Australian Rivers Institute, Griffith University, Australia
mailto:m.roberts2@griffith.edu.au
orcid:0000-0003-4027-9651

5. **Matthew K. Tam**, School of Mathematics & Statistics, University of Melbourne, Australia
mailto:matthew.tam@unimelb.edu.au
orcid:0000-0002-3654-6553

6. **Dimetre Triadis**, Department of Mathematics and Statistics, La Trobe University, Australia
mailto:d.triadis@latrobe.edu.au
orcid:0000-0002-1864-8396